

# Experimental full wavefield reconstruction and band diagram analysis in a single-phase phononic plate with internal resonators

N. Kherraz<sup>a</sup>, M. Radziński<sup>b</sup>, M. Mazzotti<sup>c</sup>, P. Kudela<sup>b</sup>, F. Bosia<sup>d</sup>, A. S. Gliozzi<sup>d</sup>, D. Misseroni<sup>e</sup>, N.M. Pugno<sup>e,f</sup>, W. Ostachowicz<sup>b</sup>, M. Miniaci<sup>a,\*</sup>

*a) CNRS, Univ. Lille, Ecole Centrale, ISEN, Univ. Valenciennes, IEMN - UMR 8520, 59046, Lille cedex, France*

*b) Institute of Fluid-Flow Machinery, Polish Academy of Science, Fiszerza 14 st. 80-231 Gdańsk, Poland*

*c) Department of Mechanical Engineering, CU Boulder, 1111 Engineering Drive, UCB 427 Boulder, CO 80309, USA*

*d) Department of Applied Science and Technology, Politecnico di Torino, Corso Duca degli Abruzzi 24, 10124, Torino, Italy*

*e) Laboratory of Bio-Inspired, Bionic, Nano, Meta Materials & Mechanics, Department of Civil, Environmental and Mechanical Engineering, University of Trento, Via Mesiano77, 38123 Trento, Italy*

*f) Queen Mary University of London, School of Engineering, Materials Science, Mile End Road, London E1 4NS, UK*

---

## Abstract

Research on phononic crystal architectures has produced many interesting designs in the past years, with useful wave manipulation properties. However, not all of the proposed designs can lead to convenient realizations for practical applications, and only a limited number of them have actually been tested experimentally to verify numerical estimations and demonstrate their feasibility.

In this work, we propose a combined numerical-experimental procedure to characterize the dynamic behavior of metamaterials, starting from a simplified 2D design to a real 3D manufacturing structure. To do this, we consider a new simplified design of a resonator-type geometry for a phononic crystal, and verify its wave filtering properties in wave propagation experiments. The proposed geometry exploits a circular distribution of cavities in a homogeneous material, leading to a central resonator surrounded by thin ligaments and an external matrix. Parametric simulations are performed to determine the optimal thickness of this design leading to a large full band gap in the kHz range. Full field experimental characterization of the resulting phononic crystal using a scanning laser Doppler vibrometer is then performed, showing excellent agreement with numerically predicted band gap prop-

---

\*correspondence to: Marco Miniaci, tel +39 329 22 59 031, email: marco.miniaci@univ-lille.fr  
Preprint submitted to Elsevier January 7, 2021

32 erties and with their resulting effects on propagating waves. The outlined procedure can  
33 serve as a useful step towards a standardization of metamaterial development and validation  
34 procedures.

35 *Keywords: Phononic Crystals, Elastic Metamaterials, Elastic Wave Propagation,*  
36 *Experimental Full Wavefield Reconstruction, Wavenumber-Frequency Analysis*

---

## 37 1. Introduction

38 The investigation of elastic wave propagation phenomena in artificially structured com-  
39 posite materials is an active research topic in the scientific community. Shortly after the  
40 introduction of photonic crystals and electromagnetic metamaterials, their elastic counter-  
41 part, i.e., phononic crystals (PCs) and elastic metamaterials [1–3], have attracted increasing  
42 attention due to the possibility of reproducing in elasticity an abundant set of unusual phys-  
43 ical properties [4], such as stop-band filtering [5, 6], negative refraction [7–9], acoustic lens-  
44 ing [10], ordinary [11, 12] and topologically protected [13–17] wave localization / splitting,  
45 and fluid elasticity [18]. Among these, the ability to attenuate elastic waves over entire fre-  
46 quency ranges, often referred to as phononic band gaps (BGs), is among the most attractive  
47 and studied properties. BGs occur due to three main mechanism: Bragg scattering, local  
48 resonance and inertial amplification [19–27].

49 Due to this property, phononic plates received great attention because of their potential  
50 for technological applications: structural health monitoring [28, 29], wave switching [30] and  
51 demultiplexing [31], micro-electro-mechanical systems [32, 32], cloaking [33], to cite a few.  
52 Among the possible configurations, phononic plates made of single or multiple constituents  
53 have been considered, including periodic distributions of inclusions, pillars / gratings on the  
54 plate surfaces, and empty holes [34].

55 In multi-material phononic plates, the shape, material type as well as the orientation of  
56 the inclusions strongly influence the existence and location in frequency of the BGs. The  
57 possibility to open both Bragg and locally resonant BG types was reported [35–37]. In single  
58 phase phononic crystals, it was shown that the local resonance of the pillars / inclusions was  
59 the dominant mechanism to open / shift BGs [38, 39]. Plates with a periodic grating on the  
60 surface have also been investigated, and a relationship established between the width of the

61 BG and the depth of the grooves [40]. While these two approaches inevitably lead to some  
62 geometrical / manufacturing complexity, phononic plates realized by through-the-thickness  
63 cavities in a homogeneous material remain a good compromise between a simpler fabrication  
64 procedure and good wave attenuation performance. Whilst numerical / theoretical works  
65 dealing with cavities perpendicular to the wave propagation plane are numerous, experimen-  
66 tal measurements are often limited to few measurement points or small scanning regions. Our  
67 aim in this paper is thus to propose an in-depth numerical and experimental characterization  
68 procedure to validate metamaterial designs and develop them into functioning realistic struc-  
69 tures. Inspired by the 2D geometry proposed for the first time by Bigoni and coworkers [10],  
70 here, we first investigate the influence of extending the design into a 3D realistic single-phase  
71 phononic plate with internal resonators generated by symmetrically arranged cavities, and  
72 then provide experimental evidence of a complete BG in the kHz frequency range. Full wave-  
73 field reconstruction of the wave propagation phenomena and a band diagram analysis in the  
74 wavenumber-frequency domain is provided and compared to numerical calculations.

## 75 **2. Design of the phononic plate**

### 76 *2.1. Eigenvalue problem*

77 In this section, we numerically investigate the dispersion properties of a periodic structure  
78 consisting of an inertial resonator embedded in a matrix through 8 ligaments, as shown in  
79 Fig. 1A. The structure is obtained by milling 8 cavities arranged in an octagonal pattern in  
80 a homogeneous Polymethyl methacrylate (PMMA, Perspex Black from Bayer) block, which  
81 divides the cell into three regions, named matrix, ligaments and resonator, respectively. This  
82 arrangement of material and cavities represents a good alternative to multi-phase resonators  
83 often made of a heavy core (in steel, tungsten or similar heavy metals) surrounded by a soft  
84 core (rubber, for instance) and embedded in an external matrix (often a polymer) [3]. In our  
85 case, the ligaments play the role of the soft coating.

86 In-plane geometrical parameters of the unit cell are given as a function of the ligament  
87 thickness  $t = 1$  mm as follows:  $A = 19 \cdot t = 19$  mm,  $R_e = 9 \cdot t$ ,  $R_i = 4 \cdot t$ , as illustrated in  
88 Fig. 1A. These parameters have been chosen with specimen fabrication in mind (i.e., with  
89 the technical limitations of the milling process in mind). The density of PMMA is  $\rho = 1180$

90 kg/m<sup>3</sup> and the longitudinal and shear wave velocities are  $c_L = 2665$  m/s and  $c_T = 1363$  m/s,  
91 respectively.

92 As a first step, the band structures are computed considering an infinitely duplicated unit  
93 cell in a periodic square array, and considering elastic wave propagation in the linear elastic  
94 regime (under the hypothesis of small displacements). The unit cell domain is meshed by  
95 means of 8-node hexagonal elements of maximum size  $L_{FE} = 0.1$  mm, which is found to  
96 provide accurate eigensolutions up to the frequency of interest [41]. Therefore, the resulting  
97 eigenvalue problem  $(\mathbf{K} - \omega^2\mathbf{M})\mathbf{u} = \mathbf{0}$  is solved by varying the non-dimensional wavevector  
98  $\mathbf{k}^*$  along the irreducible path  $[M - \Gamma - X - M]$ , with  $M \equiv (\pi/A, \pi/A)$ ,  $\Gamma \equiv (0, 0)$  and  
99  $X \equiv (\pi/A, 0)$  (see Fig. 1B), being  $A$  the lattice parameter, namely the unit cell side.

100 The corresponding band diagrams are presented in Fig. 2A for different height to the  
101 lattice parameter ratios  $H/A = [0.1, 0.5, 0.8, 1.0, 1.2]$ . The dispersion curves are color coded  
102 according to the height  $H$  of the unit cell. Specifically, the color bar of Fig. 2A varies gradually  
103 from dark blue (very thin unit cells) to dark red (thicker ones). The influence of the unit  
104 cell height on the dispersion curves is clearly visible from the diagrams. When an extremely  
105 flexible unit cell in the out-of-plane direction is considered (very small  $H/A$  ratio, for instance  
106 0.1), no complete BG is visible in the diagram. This is due to a very low stiffness of the  
107 unit cell with respect to out-of-plane deformations, implying a large number of dispersion  
108 branches in the  $[0 - 70]$  kHz frequency range. When the height to the lattice parameter  
109 ratio  $H/A$  increases, the structure gains stiffness against out-of-plane deformations and some  
110 of the previous modes migrate to higher frequencies. As a consequence, fewer curves are  
111 visible in the diagram in the same frequency range (compare for instance  $H/A = 0.1$  to  
112  $H/A = 0.5$ ). In addition, specific modes (reported in Fig. 2B,C and highlighted in Fig. 2A  
113 by black arrows), undergo an opposite shift to higher / lower frequencies. This allows to  
114 open a BG of up to 8 kHz, achieved when  $H/A = 1$ , and ranging approximately from 45  
115 to 53 kHz. If the ratio  $H/A$  increases above unity, additional bands are introduced again in  
116 the  $[0 - 70]$  kHz frequency range reducing the BG width (see for instance the flexural mode  
117 reported in Fig. 2D).

## 118 2.2. Numerical and experimental time-transient analysis on the finite structure

119 In this section, a numerical time transient analysis on a finite structure is performed, and  
120 compared to experimental measurements, as schematically indicated in Fig. 3. In view of the  
121 experimental phase, a PMMA rectangular plate of length  $4 \cdot L1 = 1000$  mm, width  $2 \cdot L1 = 500$   
122 mm and height  $H = A = 19$  mm is considered. PMMA has been chosen as the material  
123 composing both the matrix and the inertial resonators because of wide availability and the  
124 possibility of manufacturing it with standard tools such as a milling machine. A PC region  
125 made of 200 unit cells such as the one reported in Fig. 1A disposed in the shape of square  
126 rings is introduced on the right side of the plate, as shown in Fig. 3A. In particular, the unit  
127 cells are distributed over a square frame of external and internal widths of  $15A$  and  $5A$ . An  
128 unaltered area of  $5A \times 5A = 95 \times 95$  mm<sup>2</sup> is therefore included in the center of the phononic  
129 region. The sample used for the experimental analysis is manufactured by exporting the  
130 geometry from the finite element model, and importing it to the milling machine (EGX-600  
131 Engraving Machine) software.

132 The manufacturing process required a tolerance of 0.01 mm which is expected to have  
133 limited impact on the measurements.

134 Elastic guided waves are excited in correspondence of the point  $E1$  by means of a ceramic  
135 piezoelectric disk of 10 mm diameter bonded to the surface of the sample [42]. The plate  
136 has been suspended through wires to mimic the free boundary conditions implemented in  
137 the calculations. As the first step, a pulse made of 2 sine cycles centered at 50 kHz and  
138 modulated by a Hann window is fed to the function generator. This signal has been chosen  
139 so as to generate elastic waves with a much larger frequency content compared to the [45 –  
140 53] kHz frequency range of the BG highlighted in Fig. 2A. The aim is to emphasize and  
141 quantitatively evaluate the screening power of the phononic region. Out-of-plane velocity is  
142 acquired through a PSV 400 3D scanning laser Doppler vibrometer by Polytec at the two  
143 acquisition points named  $O1$  and  $O2$  (Fig. 3A), taken at the same distance from the excitation  
144 point  $E1$ , and chosen outside and inside the phononic region of the waveguide, respectively.  
145 In both cases, 3 ms long signals are recorded in order to allow multiple wave reflections to  
146 take place at both the edges of the waveguide, so as to allow elastic waves to impinge on the  
147 phononic region from multiple angles. After acquisition, signals are Fourier transformed and

148 reported in Fig. 3B in order to highlight the differences between the two responses in terms of  
149 frequency content. The Fourier spectrum of the signal acquired outside the phononic region  
150 shows good levels of transmission within the excited frequency range (30 – 90 kHz), whereas  
151 the signal recorded inside the phononic region (red markers) displays a clear amplitude drop  
152 in the BG region (45 – 53 kHz). This is in agreement with the dispersion diagram presented in  
153 Fig. 2A and clearly confirms the possibility of the waveguide to filter waves over the [45 – 53]  
154 kHz frequency range.

155 To gain further insights, full wave field reconstructions of the wave propagation phe-  
156 nomena over the orange rectangular area shown in Fig. 3A are performed and compared to  
157 numerical calculations. In the numerical model, elastic waves are excited by means of an  
158 out-of-plane imposed displacement (of amplitude  $1 \times 10^{-6}$  mm). At this stage, in addition  
159 to the previously described excitation, another pulse made of 21 sine cycles centered at 50  
160 kHz and modulated by a Hann window is used as the excitation signal fed to the function  
161 generator (and as the imposed displacement in the numerical model). In both cases, the  
162 spatial scanning grid (orange rectangle in Fig. 3A) covers a  $580 \times 500$  mm<sup>2</sup> of the right part  
163 of the phononic plate and consists of  $293 \times 251$  equally spaced grid points. A total of 10 time  
164 averages were performed at each node to increase the signal to noise ratio. The knowledge of  
165 the velocity time histories at all grid points allows for the reconstruction of the time-evolving  
166 wavefields established in the scanning domain. Figures 3C,D show the numerical (left panels)  
167 and experimental (right panels) full wavefield reconstructions of the out-of-plane velocity for  
168 the Hann windowed excitation signals using 2 (Fig. 3C) and 21 (Fig. 3D) sine cycles centered  
169 at 50 kHz fed in  $E1$ . The out-of plane velocities are normalized with respect to the respective  
170 maximum amplitudes. When operating with elastic waves with a broadband energy content,  
171 the laser measures transmission inside the phononic region, allowing the wavefield reconstruc-  
172 tion at a comparable intensity scale with respect to points of the plate not enclosed by the  
173 phononic region. However, unit cells scatter the wave field, resulting in an observable delay  
174 in the wave propagation. In this case, despite the scattering, the phononic region does not  
175 cause significant attenuation of the wave field. On the contrary, when observing the prop-  
176 agation of an elastic wave with a narrowband energy content totally falling inside the BG,  
177 strong destructive interferences due to the Bragg scattering are visible within the phononic

178 region, clearly showing that waves are reflected between the transducer and the lower edge  
179 of the unit cell ring. This behavior is accompanied by an extremely low transmission due to  
180 the absence of detectable wave amplitudes inside the phononic region.

181 As a final experiment, elastic guided waves are excited in correspondence of the point  
182 *E2*. Among several types of excitation (larger number of cycles, other waveform shapes  
183 [triangular-like, chirp-like], central frequency), the function generator has been fed with a  
184 pulse made of 2 sine cycles centered at 40 kHz and modulated by a Hann window, which  
185 showed to better inject energy in the system for the considered frequencies (also outside the  
186 BG).

187 Out-of-plane velocity is measured along 647 equally spaced points (red dashed line re-  
188 ported in Fig. 3A). Measurements are plotted as a function of the scanning position along  
189 the scan line (x-axis) and time (y-axis) in Fig. 4A, where straight red lines denote the begin-  
190 ning and the end of the periodic region. Several reflections due to the impedance mismatch  
191 are clearly visible. Signals are then 2D-Fourier transformed and reported in Fig. 4B as an  
192 intensity plot, superimposing the numerical dispersion curves as red dots for the purpose  
193 of comparison [28, 43]. A very good agreement is found. Due to the type of experimental  
194 set-up, mainly out-of plane modes are excited.

### 195 **3. Conclusions**

196 In this paper, we have presented a combined numerical and experimental characteriza-  
197 tion procedure to validate metamaterial designs to create realistic functional wave-filtering  
198 structures. We have considered an optimized design with respect to the plate thickness for  
199 a phononic crystal characterized by full BGs in the kHz range, and fully demonstrated its  
200 efficiency in wave propagation experiments. The design itself can be useful addition to other  
201 architectures considered in the literature presenting wide BGs, with the additional advantage  
202 of a simple fabrication process, e.g. by milling. More importantly, the presented experimen-  
203 tal characterization procedure can serve as a general method for standardized testing and  
204 evaluation of phononic crystal designs. To the best of our knowledge, this is the first work

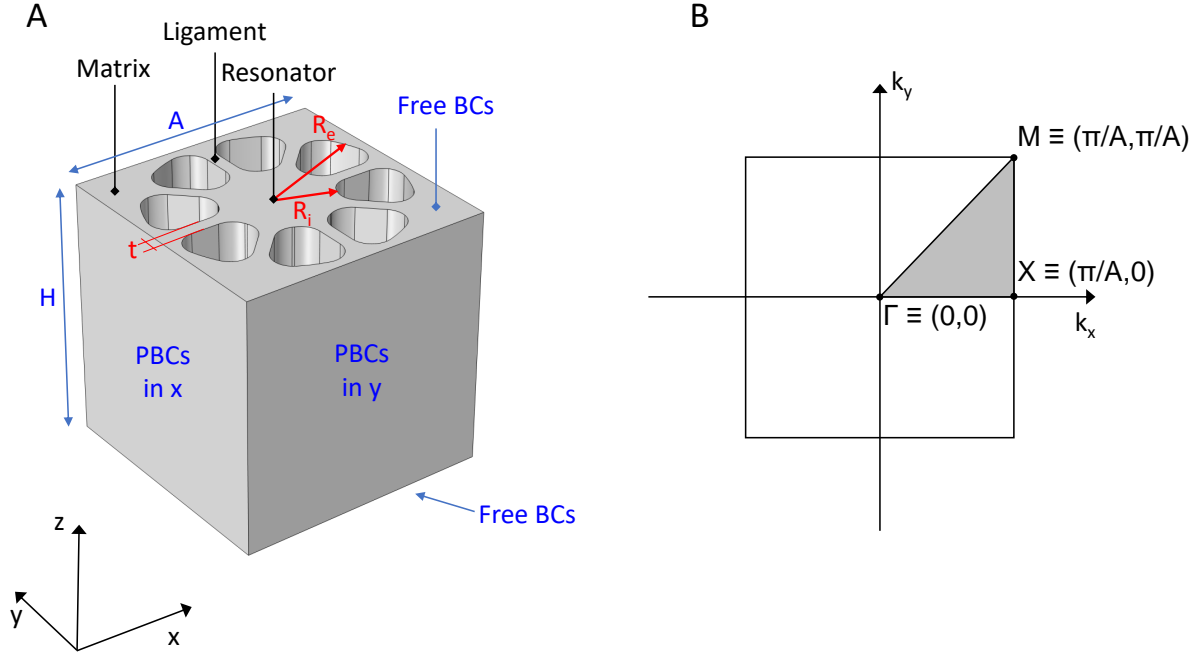


Figure 1: (A) Three-dimensional schematic representation of the unit cell investigated in this study. The structure is obtained by drilling eight cavities arranged in an octagonal pattern in a homogeneous block. The cell is thus divided into three regions, named matrix, ligaments and resonator, respectively. Geometrical parameters are the following: unit cell lattice parameter  $A = H = 19$  mm, internal and external cavity radii  $R_i = 4t$  and  $R_e = 9t$ , respectively, and ligament thickness  $t = 1$  mm. (B) Schematic representation of the first irreducible Brillouin zone along the which the dispersion curves are calculated.

205 to provide full experimental characterization for this type of geometry.

## 206 Acknowledgments

207 This project has received funding from the European Union's Horizon 2020 research and  
 208 innovation programme under grant agreement No. 863179.

## 209 References

210 [1] Rosa Martínez-Sala, J Sancho, Juan V Sánchez, Vicente Gómez, Jaime Llinares, and  
 211 Francisco Meseguer. Sound attenuation by sculpture. *Nature*, 378(6554):241–241, 1995.



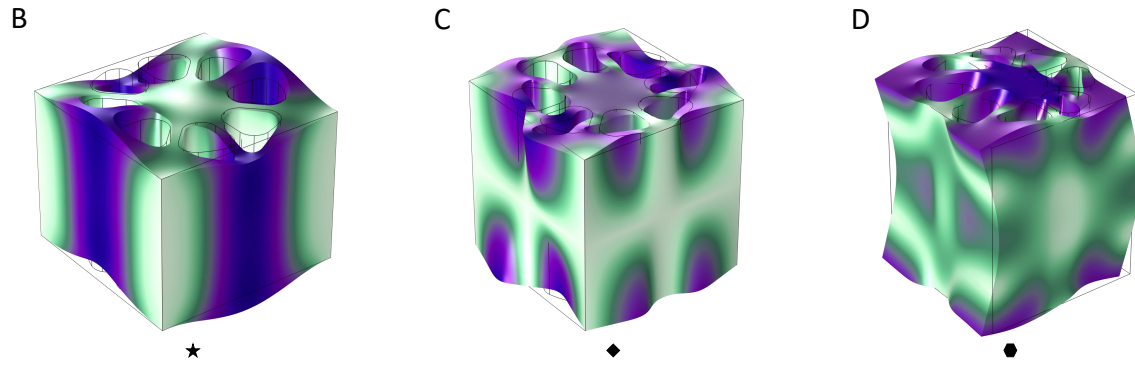
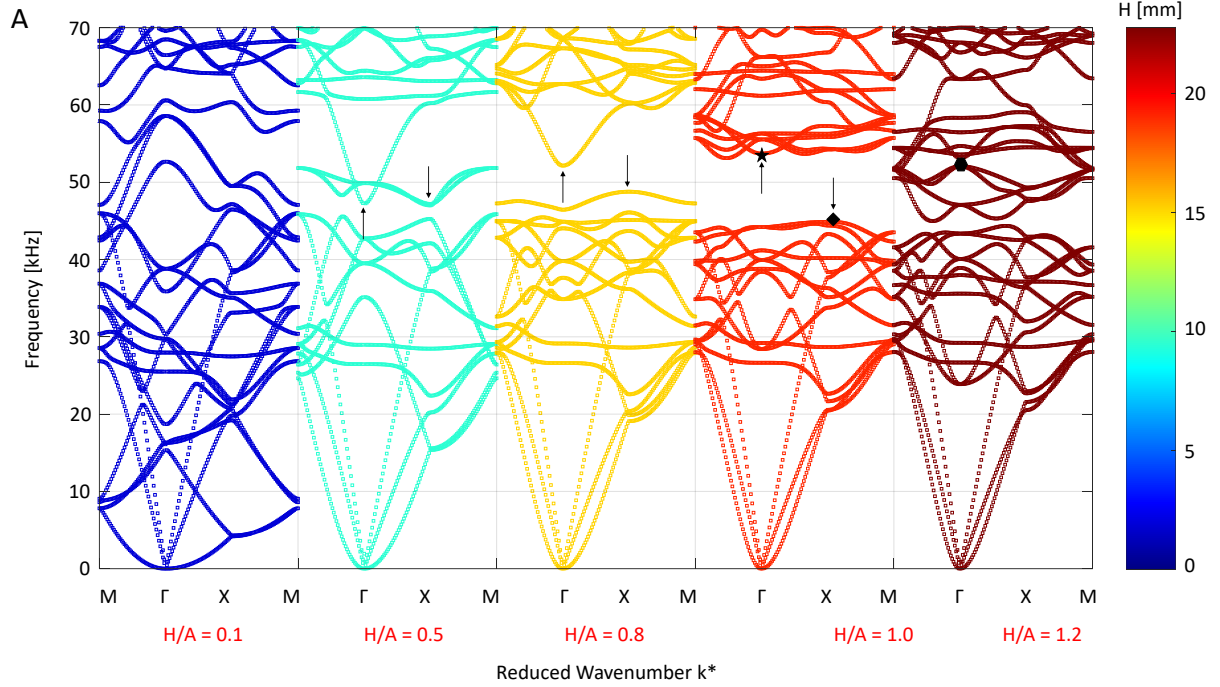


Figure 2: (A) Band diagrams along the  $M - \Gamma - X - M$  Brillouin path for the unit cell reported in Fig. 1A presented as a parametric study for different height to lattice parameter ratios  $H/A = [0.1, 0.5, 0.8, 1.0, 1.2]$ . Curves are color coded according to the height  $H$  of the unit cell, and range from dark blue (for very thin unit cells) to dark red (for the thicker ones). The influence of the height in the opening of a BG is clearly visible. When the ratio is very small  $H/A = 0.1$ , no BG is present in the diagram. This is due to the extremely flexible out-of-plane properties of the unit cell, implying a large number of vibration modes in the  $[0 - 70]$  kHz frequency range. When the height to lattice parameter ratio increases, fewer curves are visible in the diagram and in particular specific modes (highlighted by the black arrows) undergo a frequency shift in opposite directions. This allows to open a BG that increases its width up to a maximum width of 8 kHz achieved when  $H/A = 1$ . If the ratio increases above unity, additional flexural modes tend to reduce the BG width. (B-D) Deformation of the mode shapes undergoing selective frequency down(up) shift, indicated by a black star and rhombus, and located at the edges of the BG. The additional flexural mode reducing the BG width is also reported as black hexagonal marker. These modes are plotted at the  $\Gamma$  and  $X$  symmetry points. Color map indicates displacement magnitude.

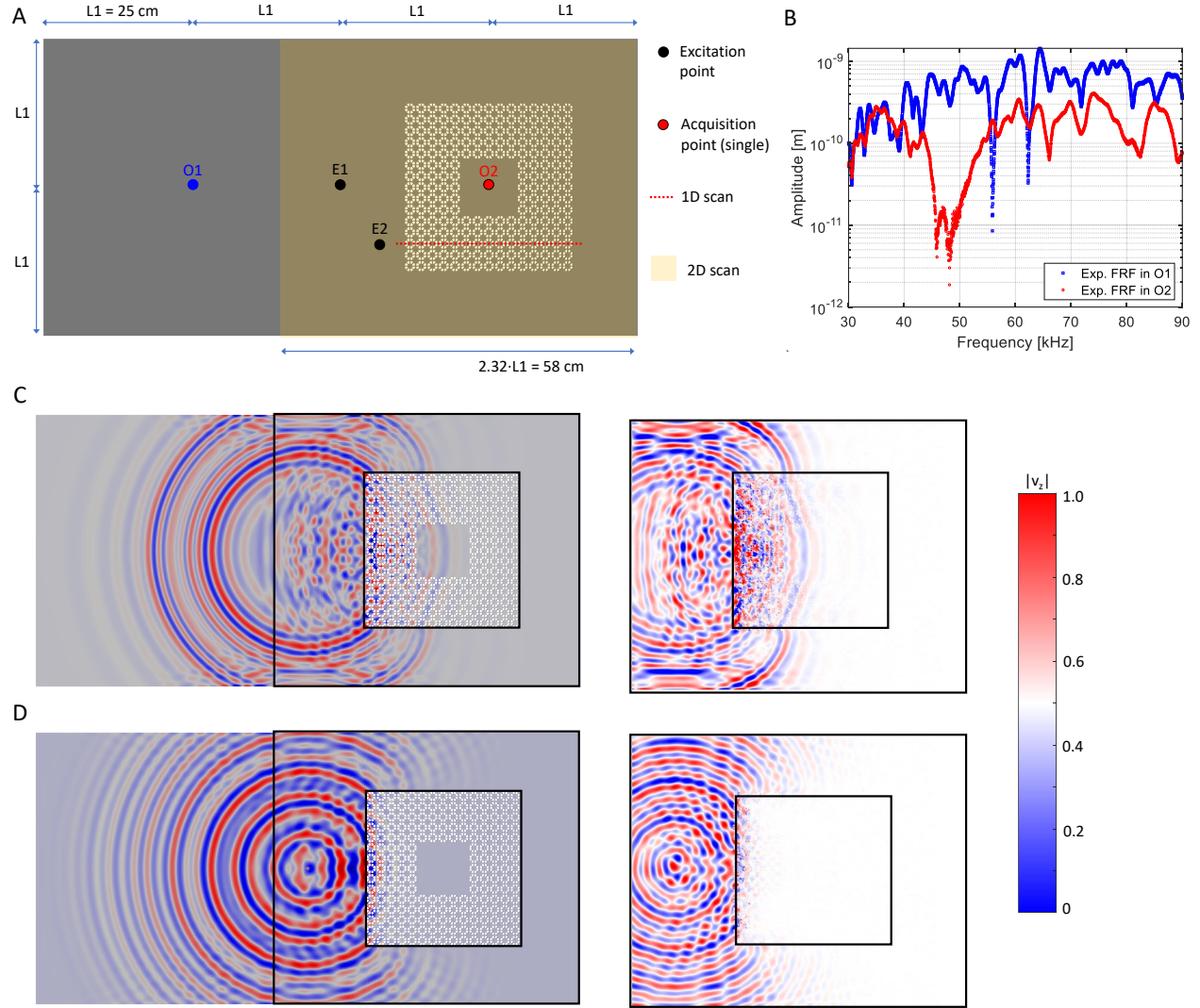


Figure 3: (A) Schematic representation of the FE model used for the three-dimensional transient dynamic computation. The specimen consists of a PMMA rectangular plate of length  $4 \cdot L1 = 1000$  mm, width  $2 \cdot L1 = 500$  mm and height  $H = A = 19$  mm), where 200 unit cells have been drilled in the shape of a square ring. Excitation points are highlighted as black dots. Measurements are performed through Scanning Laser Doppler Vibrometry in specific points outside (blue dot named  $O1$ ) and inside (red dot named  $O2$ ) the phononic ring, along a 1D line scan (dotted red line), and in a 2D region scan (orange rectangle superimposed to the schematics of the plate). (B) Frequency Response Function (FRF) of the system in the  $O1$  and  $O2$  measurement points, both located at  $L1$  from the  $E1$  excitation point. A clear drop in the amplitude is visible in the frequency domain for the measurement inside the phononic region. Numerical (left panel) and experimental (right panel) full wavefield reconstructions of the out-of-plane velocity for a (C) 2 and a (D) 21 sine cycles centered at 50 kHz Hann windowed excitation signals fed in  $E1$ . A color map of the out-of plane velocity is reported on the right, and normalized with respect to the maximum displacement.

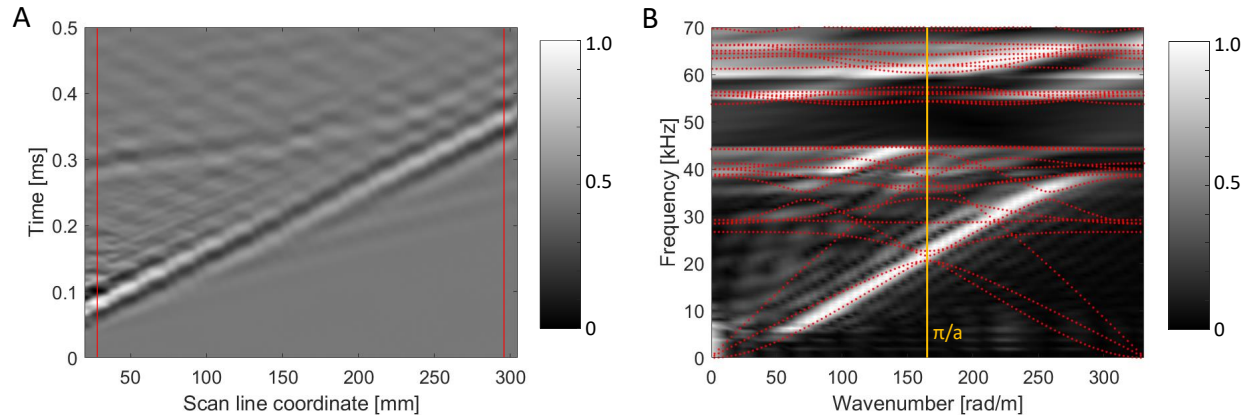


Figure 4: (A) Measured out-of-plane velocity as a function of the scanning position along the dotted red line in Fig. 3 (x-axis) and time (y-axis). Elastic waves are excited at point  $E2$  using a 2 sine cycles centered at 40 kHz and Hann windowed. Red lines denote the beginning and the end of the periodic region. Several reflections due to the impedance mismatch are clearly visible. (B) Wavenumber-frequency representation of the measured signals. Numerical dispersion curves are superimposed to the experimental results as red dots. Due to the type of experimental set-up, mainly out-of plane modes are excited.

- 212 [2] Pierre A Deymier. *Acoustic metamaterials and phononic crystals*, volume 173. Springer  
 213 Science & Business Media, 2013.
- 214 [3] Zhengyou Liu, Xixiang Zhang, Yiwei Mao, Y. Y. Zhu, Zhiyu Yang, C. T. Chan, and  
 215 Ping Sheng. Locally resonant sonic materials. *Science*, 289(5485):1734–1736, 2000.
- 216 [4] Guancong Ma and Ping Sheng. Acoustic metamaterials: From local resonances to broad  
 217 horizons. *Science advances*, 2(2):e1501595, 2016.
- 218 [5] JO Vasseur, Pierre A Deymier, B Chenni, B Djafari-Rouhani, L Dobrzynski, and D Pre-  
 219 vost. Experimental and theoretical evidence for the existence of absolute acoustic band  
 220 gaps in two-dimensional solid phononic crystals. *Physical Review Letters*, 86(14):3012,  
 221 2001.
- 222 [6] Marco Miniaci, Alessandro Marzani, Nicola Testoni, and Luca De Marchi. Complete  
 223 band gaps in a polyvinyl chloride (pvc) phononic plate with cross-like holes: numerical  
 224 design and experimental verification. *Ultrasonics*, 56:251–259, 2015.
- 225 [7] Bruno Morvan, Alain Tinel, Anne-Christine Hladky-Hennion, Jérôme Vasseur, and

- 226 Bertrand Dubus. Experimental demonstration of the negative refraction of a trans-  
227 verse elastic wave in a two-dimensional solid phononic crystal. *Applied Physics Letters*,  
228 96(10):101905, 2010.
- 229 [8] J Pierre, O Boyko, L Belliard, JO Vasseur, and Bernard Bonello. Negative refraction  
230 of zero order flexural lamb waves through a two-dimensional phononic crystal. *Applied*  
231 *Physics Letters*, 97(12):121919, 2010.
- 232 [9] Victor M García-Chocano, Johan Christensen, and José Sánchez-Dehesa. Negative re-  
233 fraction and energy funneling by hyperbolic materials: An experimental demonstration  
234 in acoustics. *Physical review letters*, 112(14):144301, 2014.
- 235 [10] Davide Bigoni, Sébastien Guenneau, Alexander B Movchan, and Morvan Brun. Elas-  
236 tic metamaterials with inertial locally resonant structures: Application to lensing and  
237 localization. *Physical Review B*, 87(17):174303, 2013.
- 238 [11] Abdelkrim Khelif, Mikael Wilm, Vincent Laude, Sylvain Ballandras, and B Djafari-  
239 Rouhani. Guided elastic waves along a rod defect of a two-dimensional phononic crystal.  
240 *Physical Review E*, 69(6):067601, 2004.
- 241 [12] G Bordiga, L Cabras, D Bigoni, and A Piccolroaz. Free and forced wave propagation in a  
242 rayleigh-beam grid: flat bands, dirac cones, and vibration localization vs isotropization.  
243 *International Journal of Solids and Structures*, 161:64–81, 2019.
- 244 [13] S Hossein Mousavi, Alexander B Khanikaev, and Zheng Wang. Topologically protected  
245 elastic waves in phononic metamaterials. *Nature communications*, 6(1):1–7, 2015.
- 246 [14] Raj Kumar Pal and Massimo Ruzzene. Edge waves in plates with resonators: an elastic  
247 analogue of the quantum valley hall effect. *New Journal of Physics*, 19(2):025001, 2017.
- 248 [15] Marco Miniaci, RK Pal, B Morvan, and M Ruzzene. Experimental observation of topo-  
249 logically protected helical edge modes in patterned elastic plates. *Physical Review X*,  
250 8(3):031074, 2018.

- 251 [16] Marco Miniaci, Raj Kumar Pal, Raffaele Manna, and Massimo Ruzzene. Valley-based  
252 splitting of topologically protected helical waves in elastic plates. *Physical Review B*,  
253 100(2):024304, 2019.
- 254 [17] Chun-Wei Chen, Natalia Lera, Rajesh Chaunsali, Daniel Torrent, Jose Vicente Alvarez,  
255 Jinkyu Yang, Pablo San-Jose, and Johan Christensen. Mechanical analogue of a majorana  
256 bound state. *Advanced Materials*, 31(51):1904386, 2019.
- 257 [18] Guancong Ma, Caixing Fu, Guanghao Wang, Philipp Del Hougne, Johan Christensen,  
258 Yun Lai, and Ping Sheng. Polarization bandgaps and fluid-like elasticity in fully solid  
259 elastic metamaterials. *Nature communications*, 7(1):1–8, 2016.
- 260 [19] Massimiliano Gei, AB Movchan, and Davide Bigoni. Band-gap shift and defect-induced  
261 annihilation in prestressed elastic structures. *Journal of Applied Physics*, 105(6):063507,  
262 2009.
- 263 [20] Richard V Craster and Sébastien Guenneau. *Acoustic metamaterials: Negative refraction,  
264 imaging, lensing and cloaking*, volume 166. Springer Science & Business Media,  
265 2012.
- 266 [21] Emanuele Baravelli and Massimo Ruzzene. Internally resonating lattices for bandgap  
267 generation and low-frequency vibration control. *Journal of Sound and Vibration*,  
268 332(25):6562–6579, 2013.
- 269 [22] Mahmoud I Hussein, Michael J Leamy, and Massimo Ruzzene. Dynamics of phononic  
270 materials and structures: Historical origins, recent progress, and future outlook. *Applied  
271 Mechanics Reviews*, 66(4), 2014.
- 272 [23] S Taniker and C Yilmaz. Design, analysis and experimental investigation of three-  
273 dimensional structures with inertial amplification induced vibration stop bands. *Inter-  
274 national Journal of Solids and Structures*, 72:88–97, 2015.
- 275 [24] Matteo Mazzotti, Marco Miniaci, and Ivan Bartoli. Band structure analysis of leaky  
276 bloch waves in 2d phononic crystal plates. *Ultrasonics*, 74:140–143, 2017.

- 277 [25] Matteo Mazzotti, Ivan Bartoli, and Marco Miniaci. Modeling bloch waves in prestressed  
278 phononic crystal plates. *Frontiers in Materials*, 6:74, 2019.
- 279 [26] C Sugino, M Ruzzene, and A Erturk. Merging mechanical and electromechanical  
280 bandgaps in locally resonant metamaterials and metastructures. *Journal of the Me-*  
281 *chanics and Physics of Solids*, 116:323–333, 2018.
- 282 [27] A Bergamini, M Miniaci, T Delpero, D Tallarico, B Van Damme, G Hannema,  
283 I Leibacher, and A Zemp. Tacticity in chiral phononic crystals. *Nature communica-*  
284 *tions*, 10(1):1–8, 2019.
- 285 [28] Marco Miniaci, Antonio S Gliozzi, Bruno Morvan, Anastasiia Krushynska, Federico  
286 Bosia, Marco Scalerandi, and Nicola M Pugno. Proof of concept for an ultrasensitive  
287 technique to detect and localize sources of elastic nonlinearity using phononic crystals.  
288 *Physical review letters*, 118(21):214301, 2017.
- 289 [29] Francesco Ciampa, Akash Mankar, and Andrea Marini. Phononic crystal waveguide  
290 transducers for nonlinear elastic wave sensing. *Scientific reports*, 7(1):1–8, 2017.
- 291 [30] Antonio S Gliozzi, Marco Miniaci, Annalisa Chiappone, Andrea Bergamini, Benjamin  
292 Morin, and Emiliano Descrovi. Tunable photo-responsive elastic metamaterials. *Nature*  
293 *communications*, 11(1):1–8, 2020.
- 294 [31] Babak Rostami-Dogolsara, Mohammad Kazem Moravvej-Farshi, and Fakhroddin  
295 Nazari. Designing switchable phononic crystal-based acoustic demultiplexer. *IEEE*  
296 *transactions on ultrasonics, ferroelectrics, and frequency control*, 63(9):1468–1473, 2016.
- 297 [32] Raffaele Ardito, Massimiliano Cremonesi, Luca D’Alessandro, and A Frangi. Application  
298 of optimally-shaped phononic crystals to reduce anchor losses of mems resonators. In  
299 *2016 IEEE International Ultrasonics Symposium (IUS)*, pages 1–3. IEEE, 2016.
- 300 [33] Diego Misseroni, Daniel J Colquitt, Alexander B Movchan, Natasha V Movchan, and  
301 Ian Samuel Jones. Cymatics for the cloaking of flexural vibrations in a structured plate.  
302 *Scientific reports*, 6:23929, 2016.

- 303 [34] Marco Miniaci, Matteo Mazzotti, Maciej Radzieński, Nesrine Kherraz, Pawel Kudela,  
304 Wieslaw Ostachowicz, Bruno Morvan, Federico Bosia, and Nicola M Pugno. Experimen-  
305 tal observation of a large low-frequency band gap in a polymer waveguide. *Frontiers in*  
306 *Materials*, 5:8, 2018.
- 307 [35] Jia-Hong Sun and Tsung-Tsong Wu. Propagation of acoustic waves in phononic-crystal  
308 plates and waveguides using a finite-difference time-domain method. *Physical Review B*,  
309 76(10):104304, 2007.
- 310 [36] Yan Pennec, Jérôme O Vasseur, Bahram Djafari-Rouhani, Leonard Dobrzyński, and  
311 Pierre A Deymier. Two-dimensional phononic crystals: Examples and applications.  
312 *Surface Science Reports*, 65(8):229–291, 2010.
- 313 [37] Yuanwei Yao, Fugen Wu, Zhilin Hou, and Zhang Xin. Lamb waves in two-dimensional  
314 phononic crystal plate with anisotropic inclusions. *Ultrasonics*, 51(5):602–605, 2011.
- 315 [38] Matthieu Rupin, Fabrice Lemoult, Geoffroy Lerosey, and Philippe Roux. Experimental  
316 demonstration of ordered and disordered multiresonant metamaterials for lamb waves.  
317 *Physical review letters*, 112(23):234301, 2014.
- 318 [39] Yabin Jin, Bernard Bonello, Rayisa P Moiseyenko, Yan Pennec, Olga Boyko, and  
319 Bahram Djafari-Rouhani. Pillar-type acoustic metasurface. *Physical Review B*,  
320 96(10):104311, 2017.
- 321 [40] Maxime Bavencoffe, Anne-christine Hladky-Hennion, Bruno Morvan, and Jean-louis  
322 Izbicki. Attenuation of lamb waves in the vicinity of a forbidden band in a phononic crys-  
323 tal. *IEEE transactions on ultrasonics, ferroelectrics, and frequency control*, 56(9):1960–  
324 1967, 2009.
- 325 [41] Luca De Marchi, Alessandro Marzani, and Marco Miniaci. A dispersion compensation  
326 procedure to extend pulse-echo defects location to irregular waveguides. *NDT & E*  
327 *International*, 54:115–122, 2013.
- 328 [42] W. Ostachowicz, P. Kudela, M. Krawczuk, and A. Zak. *Guided Waves in Structures*

329 *for SHM: The Time - domain Spectral Element Method*. A John Wiley & Sons, Ltd.,  
330 publication. Wiley, 2012.

331 [43] Paweł Kudela, Maciej Radziński, and Wiesław Ostachowicz. Identification of cracks  
332 in thin-walled structures by means of wavenumber filtering. *Mechanical Systems and*  
333 *Signal Processing*, 50:456–466, 2015.